Bi-directional Kirkendall Effect in Coaxial Microtube Nanolaminate Assemblies Fabricated by Atomic Layer Deposition

Qing Peng,[†] Xiao-Yu Sun,[†] Joseph C. Spagnola,[‡] Carl Saquing,[†] Saad A. Khan,[†] Richard J. Spontak,[†,‡] and Gregory N. Parsons[†,*]

[†]Departments of Chemical & Biomolecular Engineering and [‡]Materials Science & Engineering, North Carolina State University, Raleigh, North Carolina 27695

ABSTRACT The solid-state reaction within a coaxial $Al_2O_3/ZnO/Al_2O_3$ multilayered microtubular structure can be used to prepare discrete microtube-in-microtube $ZnAl_2O_4$ spinel assemblies through a Kirkendall void production mechanism at 700 °C. In contrast with previous studies of the nanoscale Kirkendall effect, the reaction observed here proceeds through a bi-directional vacancy diffusion mechanism wherein ZnO species diffuse into inner- and outer-Al_2O_3 concentric layers, thereby resulting in vacancy supersaturation and void production between two isolated spinel microtubes. Low-temperature atomic layer deposition (ALD) of Al_2O_3 and ZnO enables the fabrication of complex coaxial multilayered microtubes with precise control of the starting film thicknesses and relative composition. When a molar excess of ZnO is present between two Al_2O_3 layers, electron microscopy images reveal incomplete ZnO consumption after annealing at 700 °C. At higher initial Al_2O_3 concentrations, however, complete reaction with ZnO is observed, and the size of the Kirkendall gap between isolated spinel microtubes appears to be directly influenced by the thickness of the intermediate ZnO layer.

S everal interesting studies have recently demonstrated that the Kirkendall effect,[1] a well-known metallurgical process involving nonequilibrium counter-diffusion of two species through an interface, can be used to produce nanoscale objects including spherical shells,[2] nanotubes,[3−9] dendrites,[10] and other structures[11] with controlled dimensions and geometries. According to this mechanism, vacancies diffusing toward the region containing faster-diffusing species can either be annihilated at dislocations or, if the density or number of defects is sufficiently low, the vacancies can become supersaturated and condense to form voids. Production of such porous nanostructures often proceeds by exposing a small colloidal or nanocrystalline structure to a species or thin film coating of a complementary reactive compound. During subsequent reaction, accumulated vacancies will condense close to the interface and within the faster-diffusing core to form Kirkendall voids. The

resulting voids can also enable surface diffusion of species, which, in turn, can accelerate the reaction kinetics.[5,6] A wide range of complementary compounds have been identified and studied with regard to Kirkendall-related nanostructures.[2−14] The solid-state reaction and diffusion process that occurs between ZnO and Al_2O_3 in the formation of $ZnAl_2O_4$ spinel is often used as a model system. For instance, quasi-one-dimensional ZnO nanowires or branched nanostructures generated by vapor-phase processes have been coated with highly conformal Al_2O_3 films of controlled thickness by atomic layer deposition (ALD).[4−8] The solid-state reaction between ZnO and Al_2O_3 progresses through fast outward diffusion of Zn or ZnO into the Al_2O_3 layer to form hollow microtubes of a single crystal or polycrystalline $ZnAl_2O_4$ spinel.[4−8]

In all prior reports of the nanoscale Kirkendall effect induced in engineered assemblies, the nanoscale crystal "substrate" and complementary reactive coating or chemical species have been physically arranged in a bilayer (*e.g.*, Al_2O_3 on ZnO) so that the counter-diffusion process yields spinel in a single solid-state reaction zone (*e.g.*, between the ZnO and Al_2O_3 layers[4−8]). In this work, we demonstrate that, by using multilayer structures fabricated by successive ALD, the Kirkendall effect can be extended to produce alloys at multiple reaction interfaces, yielding a complex arrangement of multiple, isolated layers of a single alloy product. The resultant layers of spinel demonstrate that concurrent outward and inward diffusion of a fast-diffusing species can actively participate in Kirkendall void formation. Specifically, we show that when a trilayered $Al_2O_3/ZnO/Al_2O_3$ tubular nanostructure is prepared at material volumes

that favor stoichiometric solid-state reaction, two spinel microtubes develop as a "microtube-in-microtube" structure wherein the microtubes are physically separated by a nanoscale gap (Kirkendall void). Moreover, by varying the volumes of the coreactive species available at multiple binary junctions, the extent of each reaction and the thickness of the accompanying product layer can be independently controlled. This ability to tune multiple reaction fronts in a nanoscale Kirkendall process may open new opportunities for material design and function for a range of future nanotechnologies.

RESULTS AND DISCUSSIONS

Figure 1 is a schematic diagram of the synthesis procedure, based on atomic layer deposition chemistry, developed to generate coaxial $ZnAl_2O_4$ microtubes from sequentially layered Al_2O_3 and ZnO thin films. A matrix of electrospun poly(vinyl alcohol) (PVA) microfibers (Figure 1a) constitutes the initial substrate template. The fibers are coated with a conformal film of Al_2O_3 by ALD (Figure 1b), followed by ALD of ZnO (Figure 1c) and another Al_2O_3 layer (Figure 1d) to form trilayered $Al_2O_3/ZnO/Al_2O_3$ coaxial nanostructures on a three-dimensional (3D) PVA microfiber mat. The ALD process allows the thickness of the deposited ZnO and Al_2O_3 coatings to be independently tuned with monolayer-scale precision by adjusting the number of ALD cycles used during fabrication.[15−17] After ALD film coating, the PVA core is eliminated by annealing at 450 °C in air for 12 h (Figure 1e). Alternatively, the PVA core can be dissolved in deionized (DI) H_2O at ambient temperature. After PVA removal, the free-standing nanolaminated microtubes are further annealed at 700 °C in air for an additional 12 h to induce species diffusion and solid-state reaction, as depicted in Figure 1f. The resulting unique nanostructure portrayed in Figure 1f is referred to as a "microtube-in-microtube" arrangement. Figure 1g schematically illustrates the difference between previous studies,[4−8] where the sample geometry promotes unidirectional vacancy diffusion from the slower- toward faster-diffusing species, and the present study, where a multilayer geometry enables bi-directional vacancy diffusion.

The approach used to deposit inorganic oxides on PVA microfibers, as well as the resulting film morphology and hollow microtubes, have been previously reported.[15] Microfibers of PVA coated by Al_2O_3 appear smooth and uniform, with the film thickness precisely controlled at the monolayer level and with film deposition proceeding during the first few ALD cycles without a detectible growth incubation period.[15] Figure 2 panels a and b show PVA microfibers that have been sequentially coated by Al_2O_3 (212 ALD cycles) and ZnO (112 ALD cycles). These results confirm that successive ALD preserves the original 3D morphology of an electrospun PVA microfiber mat. An enlargement of a single PVA microfiber after coating with Al_2O_3 and ZnO is pre-
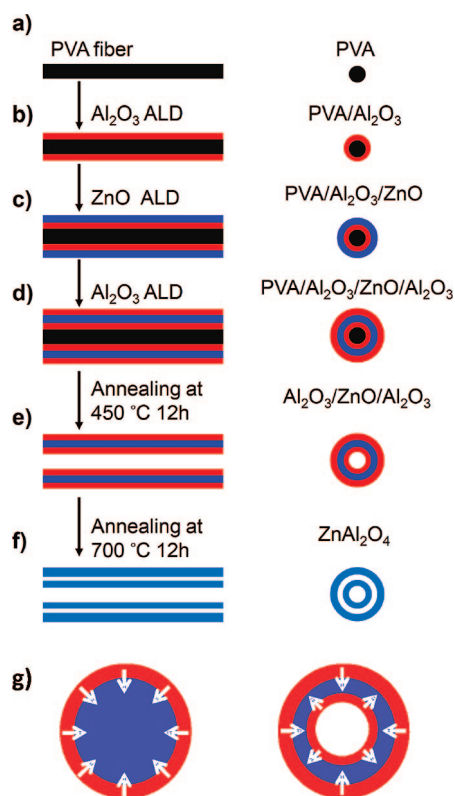
Figure 1. Schematic diagram of the procedure developed here for the fabrication of $ZnAl_2O_4$ microtube-in-microtube assemblies: (a) electrospinning is used to produce PVA microfibers; (b) a thin, conformal Al_2O_3 coating is applied to the PVA fibers by low-temperature ALD; (c) a successive ZnO coating is applied by ALD; (d) a second Al_2O_3 coating is applied by ALD, resulting in trilayered PVA/Al_2O_3/ZnO/Al_2O_3 microcables; (e) the PVA core is removed by calcination at 450 °C in air for 12 h; (f) the resultant Al_2O_3/ZnO/Al_2O_3 coaxial microtubes are annealed at 700 °C to form coaxial $ZnAl_2O_4$ microtubes separated by a nanometer-scale gap resulting from accumulation of Kirkendall voids. (g) White arrows show the direction of vacancy diffusion for a typical nanoscale Kirkendall-effect experiment in which Al_2O_3 is coated onto a ZnO crystal (left), as well as for the experimental procedure described here, where diffusion occurs in two directions to produce an internal nanoscale gap (right).

sented in Figure 2b. The dark core corresponds to the PVA microfiber with a diameter of ~300 nm, and the bright shells correspond to coaxial Al_2O_3 and ZnO coatings. Figure 2c is a TEM image of an Al_2O_3/ZnO core−shell microtube formed after dissolving the PVA substrate in DI H_2O at ambient temperature for 12 h. It is interesting to note that the PVA substrate templated in this example consisted of two parallel microfibers fused longitudinally during electrospinning, and the ALD Al_2O_3/ZnO coating accurately retains the shape of the original substrate. Because of the similar electron densities of Al_2O_3 and ZnO in this image, the precise thickness of each shell cannot be accurately determined. Similar concentric microtube morphologies are observed in all areas analyzed by TEM and are thus considered to be representative of the specimen. The surface of the outer ZnO shell is noticeably rougher than the comparable Al_2O_3 microtubes previously reported[15]
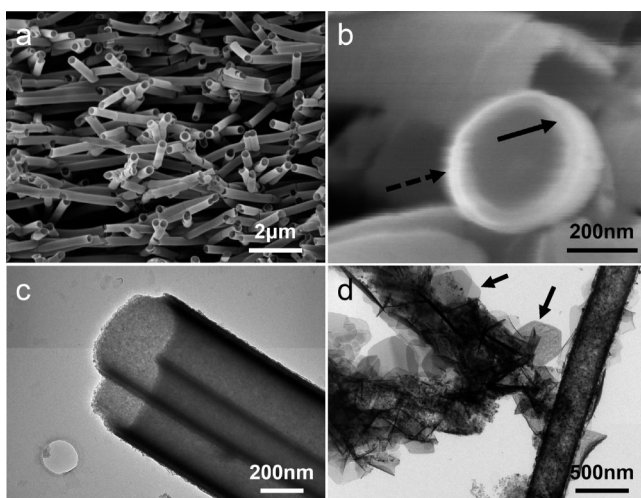
Figure 2. SEM (a and b) images of PVA electrospun fibers coated with an Al₂O₃(inner)/ZnO(outer) bilayer deposited by low-temperature ALD. Film thicknesses and the number of ALD cycles used in this and subsequent specimens are provided in 1. The SEM image in panel b shows a single PVA fiber with the coaxial bilayer coating (Al₂O₃, solid arrow; ZnO, dashed arrow). (c, d) TEM images of the coaxial Al₂O₃/ZnO microtubes obtained after removal of the PVA by dissolution in water (c) and microtubes produced after PVA calcination (d).

TABLE 1. Characteristic Dimensions of Initial ALD Layers and Post-Reaction Spinel Layers and Kirkendall Gaps[a]

figure	inner Al₂O₃	ZnO	outer Al₂O₃	spinel/gap/spinel[b]
2	18 (212)	21 (112)		
3	18 (212)	21 (112)	8.5 (100)	N/A
4	18 (212)	10 (55)	25 (300)	22 ± 0.8/6.4 ± 1.5/28 ± 1.0
5	18 (212)	21 (112)	39 (450)	23 ± 3.1/12 ± 1.8/44 ± 2.3

[a]Presented as thickness, in nm (number of ALD cycles). [b]Presented as thickness, in nm. Uncertainties represent 1 standard deviation from ~30 measurements.

to significant breakdown of the microtubular morphology. After thermal calcination at 450 °C for 12 h, followed by sonication in ethanol, the ZnO coating is found to densify as it crystallizes into microtubes composed of aggregated ZnO nanoparticles measuring 10–30 nm across. In some cases, the inner Al₂O₃ shell deteriorates to form nanoscale plates (indicated by the arrows in Figure 2d), resulting in complete disintegration of the surrounding ZnO shell. These observations are ubiquitous and representative of the specimen. It is important to note that previous studies of PVA microfibers coated only by Al₂O₃ and annealed under similar conditions in our laboratory showed no evidence of microtube disintegration.[15] The microtube deterioration exemplified in Figure 2d could be due to mechanical weak points introduced into the Al₂O₃ network by ZnO ALD. Such weak points can help to promote film disruption during thermal annealing and/or mechanical sonication.

X-ray photoelectron spectra collected from several ZnO films deposited by ALD on silicon wafers verify the presence of only Zn and O, with a relatively small amount (<2.5 atom %) of C even for films deposited at temperatures as low as 65 °C. The O1s spectrum shows evidence of oxide and O–H bonding, and peak integration indicates the –OH content comprises ~18% of the oxygen species present. Similar hydroxyl bonding is observed in infrared spectra of ZnO and Al₂O₃ layers deposited at low temperatures. We anticipate that any hydroxyl groups or carbon residue remaining after high-temperature annealing might influence the detailed energetics and kinetics of diffusion of the species/vacancy during spinel formation (e.g., by enhancing vacancy formation or species diffusion rates), but the overall reaction process should not be significantly affected.

due presumably to the crystalline nature of the ZnO ALD film. The bi/multilayered ALD coatings examined here consistently appear uniform along the length of each microtube, with no large defects detected by TEM analysis.

In the case of bilayered two-shell microtubes, removal of the PVA template by thermal calcination leads
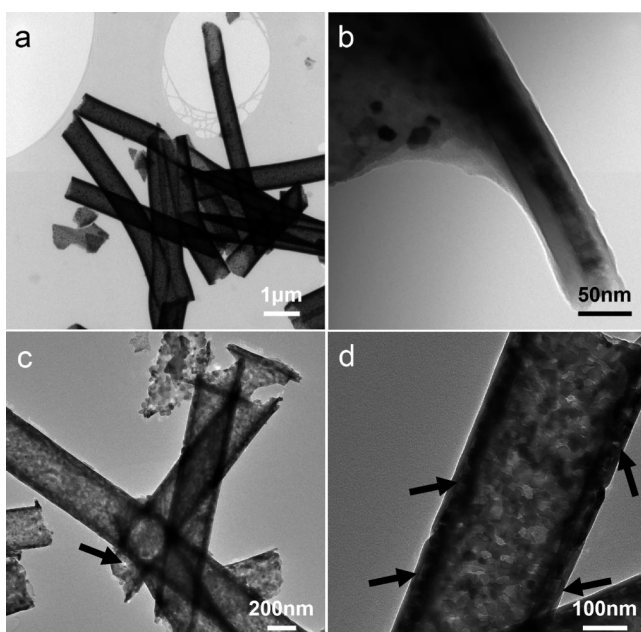
Figure 3. Representative TEM images of Al₂O₃/ZnO/Al₂O₃ microtubes formed by ALD on PVA microfibers. The images in panels a and b were obtained after annealing at 450 °C in air. The image in panel b permits direct visualization of the trilayered morphology consisting of a dark polycrystalline ZnO middle layer and lighter amorphous Al₂O₃ shells. The images in panels c and d were obtained after annealing the microtubes at 700 °C for 12 h. Light spots (arrows in c and d) indicate voids formed within the tubular structure. Unreacted excess ZnO partitions between the inner and outer shells.

To explore mechanisms related to bi-directional vacancy diffusion, trilayered specimens consisting of three chemically distinct coatings were prepared by sequential ALD, thereby forming the Al₂O₃/ZnO/Al₂O₃/PVA coaxial microfiber morphology schematically depicted in Figure 1d. Upon removal of the inner PVA core by annealing at 450 °C in air for 12 h, (cf. Figure 1e), trishell Al₂O₃/ZnO/Al₂O₃ coaxial microtubes are obtained. Transmission electron micrographs of the resulting structures obtained after low temperature annealing

are provided in panels a and b of Figures 3, 4 and 5. Each figure corresponds to samples prepared with different ALD layer thicknesses, and the number of ALD cycles used to generate each layer is listed in 1. In sharp contrast to the previous bishell microtube morphology discussed with regard to Figure 2, the images in Figures 3, 4 and 5 demonstrate significantly less disintegration (implying improved stability) when the trishell assembly is calcinated at 450 °C to eliminate the PVA core. It is reasonable to anticipate that, for the case of trishell assembly, the outer amorphous Al_2O_3 layer protects and reinforces the sandwiched semicrystalline ZnO layer. Moreover, after heating to 450 °C, the microtubes retain their compact trishell arrangement, as demonstrated, for example, in the cross-sectional, high-resolution (HR) TEM image of an Al_2O_3/ZnO/Al_2O_3 coaxial microtube displayed in Figure 3b. In this image, three clearly defined shells are evident and appear intimately bound together with no voids located between the layers. Such HRTEM images provide a direct means by which to measure the thickness of each ALD layer in the trishell assembly, and the corresponding results are included in 1. The compact arrangement of the trishell Al_2O_3/ZnO/Al_2O_3 microtube layers affords complete confinement of the middle ZnO shell, which is able to react with both the inner and outer Al_2O_3 shells to form Kirkendall voids.

Annealing the trilayered coaxial microtubes at 700 °C initiates solid-state interfacial reaction and diffusion processes, and TEM images of the resultant morphologies are also presented in Figures 3, 4, and 5. Additional HRTEM images of samples after high temperature annealing are shown in Figures 6 and 7 as well. The composite materials studied here are unique compared to previous studies of the nanoscale Kirkendall mechanism in that all of the materials involved in the reaction are strategically deposited by ALD so that the relative composition of each reactant can be readily controlled by the number of ALD cycles utilized to generate each layer. As alluded to earlier and indicated in 1, the thicknesses of the ZnO and Al_2O_3 layers are different in each of the three specimen series displayed in Figures 3, 4, and 5. Panels c and d of Figure 3 reveal that the morphology of the microtubes changes dramatically upon annealing at 700 °C for 12 h. The blotchy texture of the microtubes shown in Figure 3c suggests the formation of voids in the ZnO layer, and the TEM image provided in Figure 3d confirms the existence of Kirkendall voids in the ZnO layer below the outer Al_2O_3 shell. It is important to note that, before annealing at 700 °C, the trilayered coaxial microtubes portrayed in Figure 3 possess a ZnO/Al_2O_3 film thickness ratio of about $21/(18 + 8.2) \approx 0.80$, which is larger than the molar volume ratio $V_{ZnO}/V_{Al_2O_3}$ of $(14.5\ cm^3/mol)/(25.7\ cm^3/mol) \approx 0.56$. Although the mass density of ALD films deposited at low temperature may not be the same as bulk materials, the measured thickness ratio suggests that the sample in
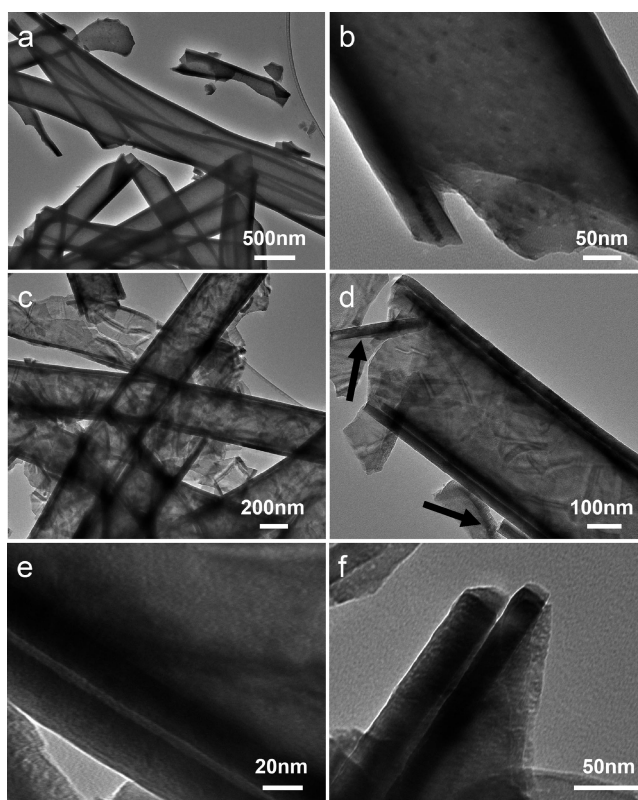
Figure 4. TEM images of Al_2O_3/ZnO/Al_2O_3 microtubes: (a, b) after annealing in air at 450 °C. The HRTEM image in panel b shows the thin dark ZnO middle layer sandwiched between two lighter Al_2O_3 layers. (c−f) After further annealing at 700 °C for 12 h. Compared to samples in Figure 3, these samples contain a thinner (∼10 nm) ZnO layer, with a thicker (∼25 nm) outer Al_2O_3 layer. The arrows in panel d identify isolated pieces of the inner or outer shells as a consequence of microtube fracture. In panels e and f, HRTEM images reveal a light middle layer located between two darker layers, indicating the formation of a thin gap between two polycrystalline $ZnAl_2O_4$ layers.

Figure 3 contained excess ZnO for the solid-state stoichiometric reaction $ZnO + Al_2O_3 \rightarrow ZnAl_2O_4$, which is consistent with the presence of ZnO after the solid-state diffusion and reaction upon annealing at 700 °C in air. For comparison, the samples discussed with regard to Figures 4 and 5 have a thinner ZnO inner shell and/or thicker Al_2O_3 outer shells, giving rise to a reaction excess of Al_2O_3 in those samples.

Figure 4 shows TEM images acquired from another set of trilayered Al_2O_3/ZnO/Al_2O_3 coaxial microtubes with film thicknesses of 18/10/25 nm, respectively. Relative to the specimen described in relation to Figure 3, this sample has a thinner (10 nm) ZnO layer and a thicker (25 nm) outer Al_2O_3 shell. Images in panels a and b of Figure 4 verify that the microtubes maintain a trilayered coaxial arrangement after calcination at 450 °C. This arrangement is particularly striking in the HR-TEM image of a broken microtube in Figure 4b, wherein the sandwiched ZnO middle layer appears dark relative to the brighter Al_2O_3 inner and outer shells. Corresponding images of microtubes annealed at 700 °C for 12 h are displayed in panels c-f of Figure 4. While broken pieces of inner and outer shells are visible in Figure
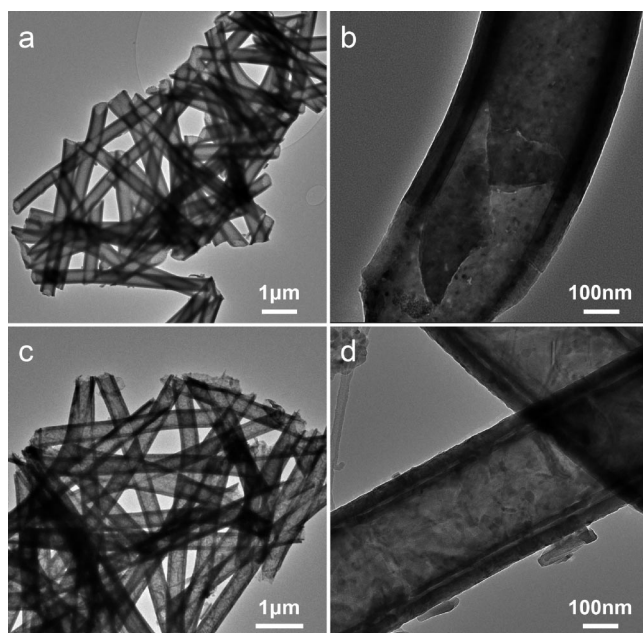
Figure 5. TEM images of Al₂O₃/ZnO/Al₂O₃ microtubes similar to those shown in Figure 4, with thicker ZnO (~21 nm) and outer Al₂O₃ (~39 nm) layers: (a, b) annealed at 450 °C in air; (c, d) annealed at 700 °C for 12 h. Image contrast (and reversal) is identical to that observed in Figure 4. A continuous Kirkendall gap is evident in panel d.

4c, panels d−f provide evidence that the trilayer morphology remains largely intact after annealing. Note, however, that the middle layer now appears bright relative to the inner and outer shells, thereby revealing a gap that develops between the two shells. Close examination of the broken microtube edge in Figure 4f confirms the presence of a gap that results from the bidirectional solid-state reaction and diffusion process between the Al₂O₃ and ZnO layers. As before, HRTEM images permit direct assessment of the thicknesses of the layers and gap, and the results are given in 1. The values reported here represent averages of more than 30 analysis points measured from several microtube samples. Two observations warrant mention here. The first is that the dimension of the gap is generally not uniform, possibly due to the relative proximity of the microtubes to each other, and surface roughness resulting from the polycrystalline nature of the inner and outer tubes. The second, expected from the solid-state reaction, is that high-temperature annealing promotes an increase in the inner and outer shell thicknesses. For the specimens shown in Figure 4, for instance, the inner shell is found to increase by 22% from 18 to ~22 nm, whereas the outer shell increases by 12% from 25 to ~28 nm. The arrow in Figure 4d identifies a broken shell piece that is ~28 nm thick. Existence of this isolated outer shell confirms that the adjacent shells are
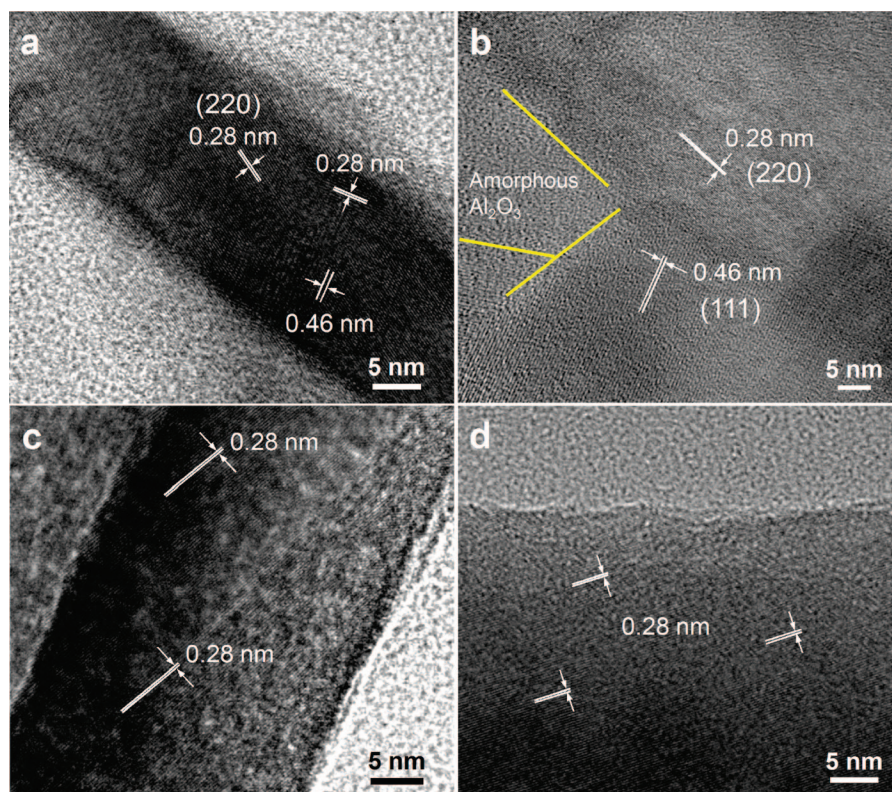

Figure 6. HRTEM images of (a) a section of an isolated inner tube wall showing polycrystalline regions, (b) a part of an inner tube shell displaying polycrystalline ZnAl₂O₄ and amorphous Al₂O₃ (outlined by yellow lines), (c) a section of an outer tube wall consisting mainly of ZnAl₂O₄ crystal, (d) a section of an outer tube wall possessing crystalline ZnAl₂O₄ and amorphous Al₂O₃. The images correspond to the inner and outer microtubes obtained from the sample shown in Figure 4. Labeled lattice spacings of 0.46 and 0.28 nm identify the 111 and 220 planes, respectively, of ZnAl₂O₄.

separated from each other after high-temperature annealing. Other broken shells from this sample set were further characterized by HRTEM, and the images are shown in Figure 6. The layers show polycrystalline domains with lattice spacings consistent with $ZnAl_2O_4$. As discussed later, X-ray diffraction data are also in agreement with this assignment. We also note from the HRTEM images in Figure 6 that the spinel $ZnAl_2O_4$ and amorphous Al_2O_3 are present as separate phases in both the inner (panels a and b) and outer (panels c and d) shells.

To further explore the versatility of this process and our capability to tune the extent of the bi-directional solid-state reaction and diffusion processes, the thickness of ZnO and Al_2O_3 shells have been further adjusted by sequential ALD to produce a larger Kirkendall gap. Images of the resulting morphologies are presented in Figure 5. Coaxial Al_2O_3/ZnO/Al_2O_3 microtubes formed after calcination are evident in panels a and b of Figure 5, while TEM images of those generated after annealing at 700 °C are included in panels c and d. After heating to 450 °C, the Al_2O_3(inner)/ZnO/Al_2O_3(outer) coaxial shells possess thicknesses of 18/21/38.5 nm, respectively, with the middle ZnO shell consistently appearing darker relative to both Al_2O_3 shells. After annealing at 700 °C, a bright gap once again appears to be sandwiched between two darker shells. This gap, particularly clear in the HRTEM image in Figure 5d, measures 11.7 ± 1.8 nm across, and the thicknesses of the outer and inner shells are 44.4 ± 2.3 nm and 22.6 ± 3.1 nm, respectively. It is important to recognize that this specimen is comparable to the sample portrayed in Figure 3 except for a thicker outer Al_2O_3 shell (38.5 versus 8.5 nm). The thicker Al_2O_3 shell allows consumption of all available ZnO during the solid-state reaction and diffusion processes upon annealing at 700 °C, thereby producing a visible gap between the spinel microtubes. This signature feature is absent in Figure 3. Densification can also be considered as a possible mechanism for void formation,[18] and the polycrystalline ZnO layers deposited at low temperature in the samples discussed with regard to Figures 3 and 5 are expected to undergo some degree of density change upon annealing. The very different final products displayed in Figures 3d and 5d cannot, however, be reconciled by considering only the densification of films. Rather, the difference between the two specimen series further corroborates the existence of a bi-directional vacancy diffusion mechanism.

The resulting physical separation between the inner and outer tubes is further visualized in the electron micrographs shown in Figure 7. These images were collected from a sample of microtubes with Al_2O_3/ZnO/Al_2O_3 of ~18/10/44 nm, respectively, after annealing at 700 °C. The electron micrograph in Figure 7a shows a broken inner tube protruding from an outer tube, demonstrating clear physical separation between the tubes.
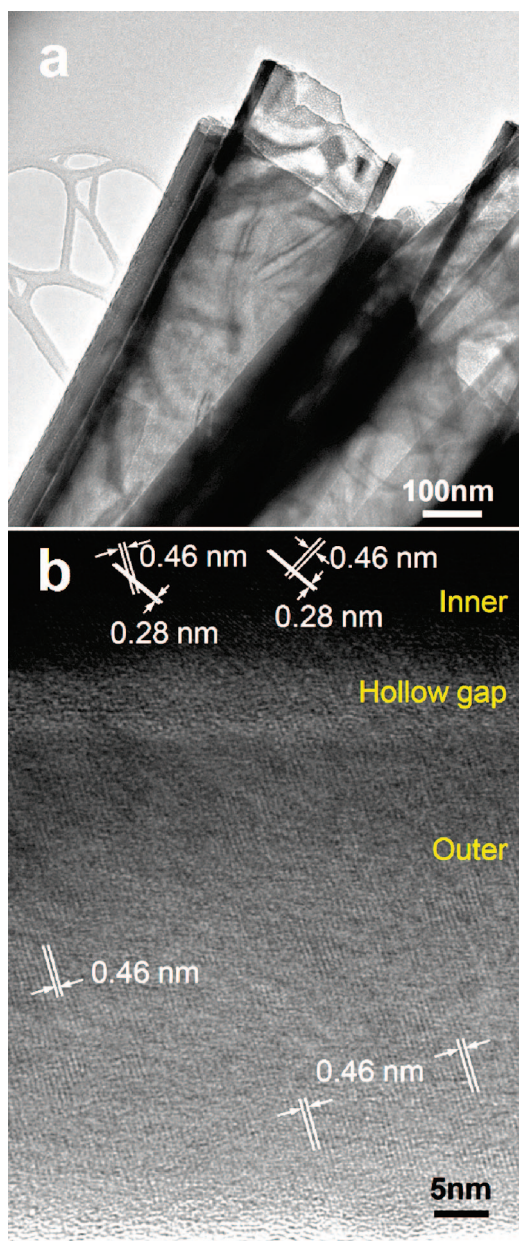
Figure 7. Typical TEM image of Al_2O_3/ZnO/Al_2O_3 microtubes (~18/10/44 nm) annealed at 700 °C for 12 h. (a) Broken tubes clearly reveal physical separation and delineation between the inner and outer spinel tubes. The image confirms increased roughness of the spinel layers along the length of the tube, on the surfaces adjacent to the Kirkendall void. A process break during the final Al_2O_3 coating step resulted in the thin line visible in the thick outer Al_2O_3 layer. (b) HRTEM image of the tubes in panel a, depicting the outer tube, hollow gap, and inner tube. The lattice spacing and orientation are consistent with polycrystalline $ZnAl_2O_4$ distributed randomly in an amorphous Al_2O_3 matrix. The lattice signal becomes weaker along the radial direction toward the outer surface of the outer shell. The width of the hollow region between the tubes is consistent with that shown in Figure 4, with a similar starting thickness of ZnO.

The size of the gap is consistent with that shown in Figure 4 for samples with a similar starting thickness of ZnO. The TEM image also shows some nanoscale roughness of the spinel layers along the length of the tube,
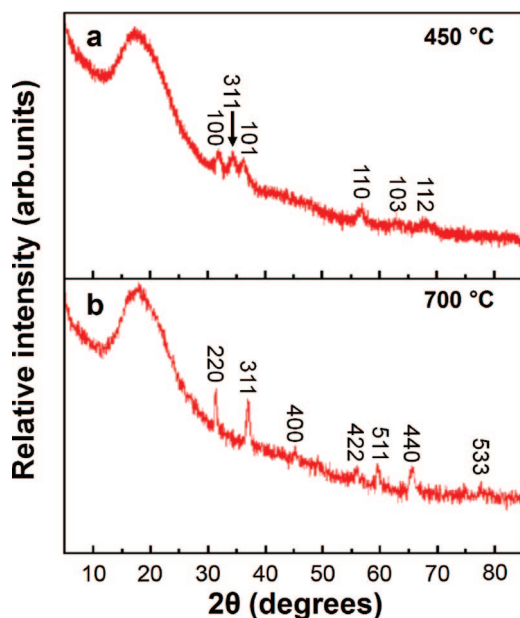
Figure 8. XRD patterns of the coaxial microtubes portrayed in Figure 4: (a) after calcination at 450 °C in air for 12 h, and (b) after annealing at 700 °C for 12 h. The reflections marked in panel a correspond to the ZnO lattice, whereas those in panel b correspond to features associated with $ZnAl_2O_4$. There is no evidence of crystalline ZnO in the diffraction pattern acquired after high-temperature annealing, which is indicative of complete reaction consumption of the ZnO layer.
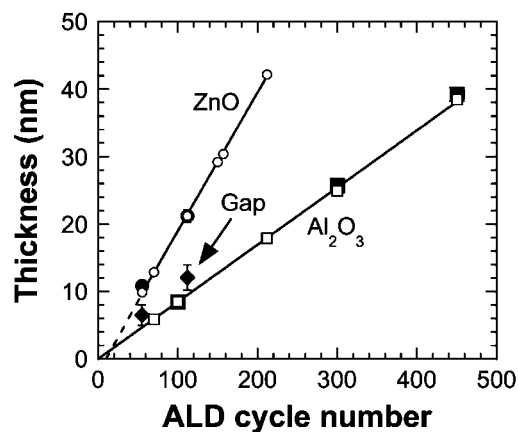

Figure 9. ALD layer thicknesses of ZnO and Al_2O_3 deposited on planar silicon wafers (measured by ellipsometry, open symbols) and microfibers (measured by TEM, filled symbols) after annealing at 450 °C in air. Included is the Kirkendall gap thickness from two Al_2O_3/ZnO/Al_2O_3 microtubular specimen series (shown in Figures 4 and 5) annealed at 700 °C and plotted as a function of the ALD cycle number for the ZnO layer. The error bars represent one standard deviation in the data.

on the surface adjacent to the Kirkendall void. The HR-TEM image in Figure 7b likewise reveals the polycrystalline nature of the tubes, consistent with inward and outward diffusion of Zn-related species into the Al_2O_3 layers. Measured lattice spacings are consistent with $ZnAl_2O_4$, and a sharp interface does not appear to exist between excess Al_2O_3 and the spinel shells.

In addition to the microtube structures shown here, it may be possible to extend the concept introduced here to planar or other three-dimensional nano- or microstructures. In a planar configuration, the bidirectional Kirkendall reaction for nanolaminated Al_2O_3/ZnO/Al_2O_3 films with suitable molar ratio is expected to result in two $ZnAl_2O_4$ layers. However there is no physical means to support a large area gap between these layers. Preliminary experiments suggest formation of two planar layers that may be physically separated by, for example, mechanical peeling.

The crystal structure of the microtubes displayed in Figure 4 have been analyzed by XRD after annealing at 450 and 700 °C, and results are provided in panels a and b, respectively, of Figure 8. The specimen annealed at 450 °C shows only ZnO-related diffraction features, consistent with polycrystalline ZnO located between amorphous Al_2O_3 layers. The reflections present after annealing at 700 °C, on the other hand, correspond to polycrystalline $ZnAl_2O_4$ spinel, providing direct evidence for the solid-state reaction between ZnO and Al_2O_3 in the coaxial microtubes assembly. In this case, the interfacial reaction appears to consume all the ZnO

reactant in the middle shell. Previous results[19−21] show that thin ALD Al_2O_3 films develop crystalline order upon extended annealing at temperatures above 800 °C. The formation of segregated interfacial voids and microtube-in-microtube structures therefore demonstrates that the nanoscale Kirkendall effect can be directly extended to trilayered systems, where the solid-state reaction and diffusion simultaneously proceeds in two opposite directions across two spatially isolated interfaces.

The results shown in Figure 9 for samples in the microtube geometry highlight the ability to tune the thickness of deposited films by sequential ALD and the size of the reaction-induced Kirkendall gap that can develop between microtubes. The figure compares the thicknesses of ALD coatings in microtube assmblies, as measured by TEM after annealing at 450 °C, to those of ALD films deposited directly on planar silicon wafers, as determined by ellipsometry. As expected, the thickness of the ZnO and Al_2O_3 films deposited on a planar surface increases linearly with the number of ALD cycles at a growth rate of ∼0.19 nm/cycle for ZnO and ∼0.08 nm/cycle for Al_2O_3. Several cycles of growth incubation time may be required for ZnO ALD, which is consistent with previous reports.[16,22] The TEM results gleaned from layers deposited under the same conditions on the fiber matrix indicate remarkably similar growth rates. The TEM data constitute mean values of more than 30 measurements, and the corresponding standard deviation is less than 7% on average. Figure 9 also shows the size of the gap between microtubes after annealing at 700 °C. These results, obtained from TEM images such as those provided in Figures 3, 4, and 5, are plotted as a function of the cycle number used for ZnO ALD. Under conditions where there is sufficient Al_2O_3

present to react with the available ZnO (*i.e.*, the sample series displayed in Figures 4 and 5), the void dimension increases with increasing ZnO thickness, demonstrating that the Kirkendall gap size can be controlled by varying the ALD film thickness. It is important to note that the precise correspondence between the starting ZnO layer thickness and the ensuing void or gap size will depend on the reaction volume of the surrounding Al_2O_3 layers. When insufficient Al_2O_3 reactant is available and ZnO is in molar excess, discrete voids, rather than a distinct, contiguous gap, develop after annealing at 700 °C for 12 h (*cf.* Figure 3).

CONCLUSIONS

The experimental results reported here establish that Kirkendall voids can be formed between two $ZnAl_2O_4$ spinel microtubes through the solid-state reaction and diffusion processes between concentric Al_2O_3 and ZnO shells deposited by low-temperature ALD on fibrous templates. The resulting morphologies can be described as microtube-in-microtube $ZnAl_2O_4$ assemblies, where the individual spinel microtubes are separated by a continuous hollow gap. The process is understood in terms of a bi-directional vacancy diffusion mechanism, wherein ZnO diffuses into both inner and outer Al_2O_3 layers, resulting in vacancy accumulation and supersaturation between the two spinel microtubes. If the mole fraction of Al_2O_3 is insufficient for completion of the spinel formation reaction, excess ZnO crystallites remain in the reaction zone after annealing. For samples with an equal or excess Al_2O_3 mole fraction, the thickness of the Kirkendall gap between isolated spinel microtubes can be controlled in part by the thickness of the deposited ZnO layer. Fabrication of microtube-in-microtube assemblies is achieved using the precise control over layer thickness afforded by ALD of Al_2O_3 and ZnO thin layers at low deposition temperatures. This work demonstrates that complex material multilayers produced by ALD can enable vacancy diffusion in more than one direction. Extending this scheme to other materials and geometries will open new possibilities for complex nanoarchitecture synthesis and engineering in a broad range of nanotechnological applications.

METHODS

The inorganic coaxial microtubes used in this study were prepared by coating electrospun poly(vinyl alcohol) (PVA) microfibers with Al_2O_3 and ZnO thin films deposited by ALD. The fabrication processes regarding PVA electrospinning and ALD coating were described elsewhere.[15,23] In the present work, Al_2O_3 ALD was conducted at 45 °C and ~0.9 Torr.[15] A modestly higher temperature (65 °C) was used for ZnO ALD, also performed at ~0.9 Torr. The reactants included two organometallic precursors: trimethylaluminum ($Al(CH_3)_3$, TMA, 98%, Strem) and diethyl zinc ($Zn(C_2H_5)_2$, DEZ, 96%, Strem) and deionized water vapor (DI H_2O). All the species were delivered as ambient-temperature vapors into a custom-built hot-wall viscous flow tube reactor. High-purity Ar (99.999%) (National Welders Supply Co.) was used as the purge and carrier gas and further purified by a gas filter (DRIERITE Gas Purifier) before entering the reaction system. During cycling, the TMA and DI H_2O were alternately introduced into the ALD chamber (base pressure ~10^{-6} Torr) in pulses of 5 and 1 s, respectively. Corresponding purge times were 20 (TMA) and 60 s (DI H_2O). For ZnO deposition, DEZ and DI H_2O were likewise injected into the reactor in pulses of 5 and 2 s, respectively, and each purge time was 120 s. In conjunction with each ALD deposition on PVA microfiber mats, two pieces of silicon wafer (measuring ~1 cm × 1.5 cm, treated by JTB Baker Clean, rinsed in DI water, and then blown-dry with N_2) were used as reference substrates for growth rate measurements on a planar surface under identical deposition conditions. During deposition, the microfiber mat was positioned between the two Si wafers. The PVA microfiber templates were removed either by heating in air at 450 °C for 12 h or dissolution in DI H_2O for 12 h. To stimulate solid-state interfacial reaction, resultant specimens consisting of coaxial microtubes composed of Al_2O_3 and ZnO layers were subsequently annealed in a convective air furnace at 700 °C for 12 h. Microfibers and microtubes were examined by field-emission scanning electron microscopy (FESEM) performed on a JEOL 6400F microscope operated at 5 kV. Microtube samples for transmission electron microscopy (TEM) analysis were first sonicated in ethanol for 1 min. Several drops of the suspension were pipetted onto carbon-coated TEM grids, which were allowed to dry at ambient temperature and then imaged with an FEI Tecnai G^2 twin microscope operated at 160 kV. The crystal structure of the microtubes were characterized by X-ray diffractometry (XRD) performed on a Philips X'Pert PRO MRD HR diffractometer over an angular range of 5–85° (2θ) in intervals of 0.01° (2θ) and with a step duration of 1 s. For XRD, a mat of microtubes was attached to the sample holder by means of double-sided tape. The Al_2O_3 and ZnO ALD film thicknesses on Si wafer were discerned by ellipsometry using refractive indices of 1.79 and 2.00 for Al_2O_3 and ZnO, respectively. X-ray photoelectron spectroscopy (XPS) measurements were conducted on a Kratos Analytical AXIS ULTRA spectrometer outfitted with a monochromatic Al Kα source and operated at 15 kV. For all samples, the C 1s peak was normalized to 284.6 eV as the reference. In the survey and detail scans, the pass energies were maintained at 160 and 20 eV, respectively, and the data were analyzed and fitted using the CasaXPS software suite.

REFERENCES AND NOTES

1. Smigelskas, A. D.; Kirkendall, E. O. Zinc Diffusion in Alpha-Brass. *Trans. Am. Inst. Mining Metall. Eng.* **1947**, *171*, 130–142.
2. Yin, Y. D.; Rioux, R. M.; Erdonmez, C. K.; Hughes, S.; Somorjai, G. A.; Alivisatos, A. P. Formation of Hollow Nanocrystals Through the Nanoscale Kirkendall Effect. *Science* **2004**, *304*, 711–714.
3. Tu, K. N.; Gosele, U. Hollow Nanostructures Based on the Kirkendall Effect: Design and Stability Considerations. *Appl. Phys. Lett.* **2005**, *86* 093111-1–093111-3.
4. Fan, H. J.; Knez, M.; Scholz, R.; Nielsch, K.; Pippel, E.; Hesse, D.; Zacharias, M.; Gosele, U. Monocrystalline Spinel Nanotube Fabrication Based on the Kirkendall Effect. *Nat. Mater.* **2006**, *5*, 627–631.
5. Fan, H. J.; Gosele, U.; Zacharias, M. Formation of Nanotubes and Hollow Nanoparticles Based on Kirkendall

and Diffusion Processes: A Review. *Small* **2007**, *3*, 1660–1671.

6. Fan, H. J.; Knez, M.; Scholz, R.; Hesse, D.; Nielsch, K.; Zacharias, M.; Gosele, U. Influence of Surface Diffusion on the Formation of Hollow Nanostructures Induced by the Kirkendall Effect: The Basic Concept. *Nano Lett.* **2007**, *7*, 993–997.

7. Yang, Y.; Kim, D. S.; Knez, M.; Scholz, R.; Berger, A.; Pippel, E.; Hesse, D.; Gosele, U.; Zacharias, M. Influence of Temperature on Evolution of Coaxial ZnO/Al$_2$O$_3$ One-Dimensional Heterostructures: From Core-Shell Nanowires to Spinel Nanotubes and Porous Nanowires. *J. Phys. Chem. C* **2008**, *112*, 4068–4074.

8. Yang, Y.; Kim, D. S.; Scholz, R.; Knez, M.; Lee, S. M.; Gosele, U.; Zacharias, M. Hierarchical Three-Dimensional ZnO and Their Shape-Preserving Transformation into Hollow ZnAl$_2$O$_4$ Nanostructures. *Chem. Mater.* **2008**, *20*, 3487–3494.

9. Qiu, Y.; Yang, S. Kirkendall Approach to the Fabrication of Ultra-Thin ZnO Nanotubes with High Resistive Sensitivity to Humidity. *Nanotechnology* **2008**, *19*, 265606-1–265606-7.

10. Ng, C. H. B.; Tan, H.; Fan, W. Y. Formation of Ag$_2$Se Nanotubes and Dendrite-Like Structures from UV Irradiation of a CSe$_2$/Ag Colloidal Solution. *Langmuir* **2006**, *22*, 9712–9717.

11. Li, Q.; Penner, R. M. Photoconductive Cadmium Sulfide Hemicylindrical Shell Nanowire Ensembles. *Nano Lett.* **2005**, *5*, 1720–1725.

12. Yin, Y. D.; Erdonmez, C. K.; Cabot, A.; Hughes, S.; Alivisatos, A. P. Colloidal Synthesis of Hollow Cobalt Sulfide Nanocrystals. *Adv. Funct. Mater.* **2006**, *16*, 1389–1399.

13. Henkes, A. E.; Vasquez, Y.; Schaak, R. E. Converting Metals into Phosphides: A General Strategy for the Synthesis of Metal Phosphide Nanocrystals. *J. Am. Chem. Soc.* **2007**, *129*, 1896–1897.

14. Chiang, R. K.; Chiang, R. T. Formation of Hollow Ni$_2$P Nanoparticles Based on the Nanoscale Kirkendall Effect. *Inorg. Chem.* **2007**, *46*, 369–371.

15. Peng, Q.; Sun, X. Y.; Spagnola, J. C.; Hyde, G. K.; Spontak, R. J.; Parsons, G. N. Atomic Layer Deposition on Electrospun Polymer Fibers as a Direct Route to Al$_2$O$_3$ Microtubes with Precise Wall Thickness Control. *Nano Lett.* **2007**, *7*, 719–722.

16. Elam, J. W.; George, S. M. Growth of ZnO/Al$_2$O$_3$ Alloy Films Using Atomic Layer Deposition Techniques. *Chem. Mater.* **2003**, *15*, 1020–1028.

17. Elam, J. W.; Sechrist, Z. A.; George, S. M. ZnO/Al$_2$O$_3$ Nanolaminates Fabricated by Atomic Layer Deposition: Growth and Surface Roughness Measurements. *Thin Solid Films* **2002**, *414*, 43–55.

18. Striemer, C. C.; Gaborski, T. R.; McGrath, J. L.; Fauchet, P. M. Charge- and Size-Based Separation of Macromolecules Using Ultrathin Silicon Membranes. *Nature* **2007**, *445*, 749–753.

19. Jakschik, S.; Schroeder, U.; Hecht, T.; Gutsche, M.; Seidl, H.; Bartha, J. W. Crystallization Behavior of Thin ALD-Al$_2$O$_3$ Films. *Thin Solid Films* **2003**, *425*, 216–220.

20. Scarel, G.; Hyde, G. K.; Hojo, D.; Parsons, G. N. Berreman Effect in Infrared Absorption Spectroscopy of Ionic Oxide Coatings Formed by Atomic Layer Deposition on Three-Dimensional Structures. *J. Appl. Phys.* **2008**, *104*, 094314-1–094314-9.

21. Afanas'ev, V. V.; Stesmans, A.; Mrstik, B. J.; Zhao, C. Impact of Annealing-Induced Compaction on Electronic Properties of Atomic-Layer-Deposited Al$_2$O$_3$. *Appl. Phys. Lett.* **2002**, *81*, 1678–1680.

22. Yousfi, E. B.; Fouache, J.; Lincot, D. Study of Atomic Layer Epitaxy of Zinc Oxide by *in-Situ* Quartz Crystal Microgravimetry. *Appl. Surf. Sci.* **2000**, *153*, 223–234.

23. Sun, X. Y.; Shankar, R.; Börner, H. G.; Ghosh, T. K.; Spontak, R. J. Field-Driven Biofunctionalization of Polymer Fiber Surfaces during Electrospinning. *Adv. Mater.* **2007**, *19*, 87–91.